BBA - Biomembranes 1861 (2019) 335–343

Contents lists available at ScienceDirect

BBA - Biomembranes

journal homepage: www.elsevier.com/locate/bbamem

Electrophysiological interrogation of asymmetric droplet interface bilayers reveals surface-bound alamethicin induces lipid flip-flop☆

Graham Taylor[a,b,1], Mary-Anne Nguyen[a,1], Subhadeep Koner[a], Eric Freeman[c], C. Patrick Collier[d], Stephen A. Sarles[a,*]

[a] Department of Mechanical, Aerospace, and Biomedical Engineering, The University of Tennessee, Knoxville, TN 37996, United States
[b] The Bredesen Center for Interdisciplinary Research, The University of Tennessee, Knoxville, TN 37996, United States
[c] Department of Mechanical Engineering, The University of Georgia, Athens, GA, United States
[d] Center for Nanophase Materials Sciences, Oak Ridge National Laboratory, Oak Ridge, TN, 37831, United States

A B S T R A C T

The droplet interface bilayer (DIB) method offers simple control over initial leaflet compositions in model membranes, enabling an experimental path to filling gaps in our knowledge about the interplay between compositional lipid asymmetry, membrane properties, and the behaviors of membrane-active species. Yet, the stability of lipid leaflet asymmetry in DIBs has received very little attention, particularly in the presence of peptides and ion channels that are often studied in DIBs. Herein, we demonstrate for the first time parallel, capacitance-based measurements of intramembrane potential with arrays of asymmetric DIBs assembled in a microfluidic device to characterize the stability of leaflet asymmetry over many hours in the presence and absence of membrane-active peptides. DIBs assembled from opposing monolayers of the ester (DPhPC) and ether (DOPhPC) forms of diphytanoyl-phosphatidylcholine yielded asymmetric bilayers with leaflet compositions that were stable for at least 18 h as indicated by a stable |137 mV| intramembrane potential. In contrast, the addition of surface-bound alamethicin peptides caused a gradual, concentration-dependent decrease in the magnitude of the dipole potential difference. Intermittent current-voltage measurements revealed that alamethicin in asymmetric DIBs also shifts the threshold voltage required to drive peptide insertion and ion channel formation. These outcomes take place over the course of 1 to 5 h after membrane formation, and suggest that alamethicin peptides promote lipid flip-flop, even in the un-inserted, surface-bound state, by disordering lipids in the monolayer to which they bind. Moreover, this methodology establishes the use of parallel electrophysiology for efficiently studying membrane asymmetry in arrays of DIBs.

1. Introduction

The structures and functions of cells are greatly influenced by the membranes that surround the cell and envelop intracellular organelles. These membranes each consist of two leaflets primarily comprised of phospholipids. Cells actively expend energy to maintain different, or asymmetric, lipid compositions within each leaflet [1–3]. Asymmetric membrane compositions are associated with physiological functions, for example membrane protein mediated signaling pathways [3] and activation of clotting factors signaled via elevated expression of PS lipids on red blood cells [4]. Moreover, the loss of membrane asymmetry is a first step towards cell death [5]. Yet, even after several decades of biomembrane research, much remains to be understood regarding biophysical mechanisms associated with asymmetric membranes in natural cellular environments, including the interactions of membranes with proteins and peptides.

To elucidate the fundamental chemistries and biophysics relevant to leaflet asymmetry, researchers have developed techniques to assemble and experimentally characterize spherical and planar model membranes with leaflet asymmetry [3]. For example, unilamellar liposomes with asymmetric leaflet compositions can be obtained using multiphase droplet transfer [6,7], jetting microfluidics through a planar bilayer [8–11], and cyclodextrin (CD) mediated exchange [12,13] between the outer leaflets of symmetric donor and accepter liposomes having different compositions. Despite their value, these approaches require sophisticated microfluidic systems or time-consuming mixing, incubation, washing, and purification steps to achieve asymmetric membranes. The closed-sphere liposome geometry also complicates the

* Corresponding author at: Bioinspired Materials and Transduction Laboratory, Department of Mechanical, Aerospace, and Biomedical Engineering, University of Tennessee, Knoxville, Knoxville, TN 37996, United States.
E-mail address: ssarles@utk.edu (S.A. Sarles).
[1] Co-first authors.

https://doi.org/10.1016/j.bbamem.2018.07.001
Received 20 March 2018; Received in revised form 6 July 2018; Accepted 9 July 2018
Available online 10 July 2018
0005-2736/

use of electrophysiology for quantifying membrane properties, protein and peptide activity, and ion transport [14]. Further, peptide-enhancement of lipid flip-flop in asymmetric liposomes has been characterized using fluorescence quenching by incorporating probe-modified lipids [15, 16] as well as via neutron scattering measurements on vesicles incorporating deuterated lipids [17]. Separately, asymmetric solid-supported planar bilayers have been created via Langmuir-Blodgett/Schäfer or Langmuir-Blodgett/vesicle fusion techniques [18–30], while asymmetric suspended lipid bilayers (i.e. Black Lipid Membranes (BLMs)) [31–37] can be constructed using the lipid folding method introduced by Montal and Mueller [38]. And while these systems permit imaging and electrophysiological characterization of bilayers, respectively, they too have drawbacks. The underlying solid substrate can affect lateral diffusion and *trans*-leaflet kinetics of lipids in supported membranes [13,39], and BLMs require significant skill to assemble and are notoriously fragile, which limits their lifetimes of use.

In contrast, the DIB technique [40–43] for constructing a planar bilayer between lipid-coated aqueous droplets in oil offers controlled assembly of membranes (i.e. *DIBs*) with asymmetric leaflets by incorporating liposomes of different types into separate droplets [44]. The DIB approach not only preserves the ability to conduct electrical measurements on membranes and obviates the need for a supporting substrate, but it also results in stable membranes that can be studied for hours to weeks [43] and uniquely allows for creating large bilayer arrays and interconnected networks (in 2D and 3D) between many droplets [45].

However, only a handful of studies to-date have used DIBs to explore biophysical questions about membrane asymmetry. Hwang et al. reported that headgroup charge asymmetry in DPhPC leaflets doped with either dipalmitoyl phosphatidylglycerol (DPPG, "−") or dimethyldioctadecylammonium bromide (DDAB, "+") affected the gating behavior of OpmG porins from *E. coli* [43]. Milianta et al. distributed sterols asymmetrically in DIBs for the purpose of understanding how leaflet asymmetry affects the permeability of a membrane to water [46]. Barlow et al. constructed plant-inspired DIBs with asymmetrically distributed lipids, sterols, and cerebrosides and used a dye leakage assay to quantify the stability and permeability of asymmetric model membranes versus composition [47]. Separately, Barlow, et al. recently assessed the effects of the unstirred water layer on membrane permeability using asymmetric DIB leaflets comprised of mixtures of lipids [48]. Finally, Freeman et al. investigated the effect of a non-zero intramembrane potential on mechanotransduction, including flexoelectricity, in DIBs constructed from asymmetric leaflets of 1,2 diphytanoyl-*sn*-glycero-3-phosphocholine (DPhPC) and 1,2-di-O-phytanoyl-*sn*-glycero-phosphocholine (DOPhPC) lipids [49].

Important details regarding the interplay between compositional lipid asymmetry, membrane properties, and the behaviors of membrane-active species in DIBs remain poorly understood. For example, no studies have quantitatively tracked lipid asymmetry in DIBs over time or explored lipid translocation (i.e. flip-flop) in the presence of small, membrane-active peptides, such as alamethicin. Further, while Hall studied the effect of intramembrane surface potential caused by headgroup charge asymmetry on alamethicin ion channel conductance in BLMs [50], there are no reports about the effects of a sub-surface transmembrane dipole potential on the voltage-activated insertion of alamethicin peptides. Therefore, we propose that additional studies are needed to understand the stability of lipid asymmetry in DIBs and probe the two-way effects of voltage-dependent membrane-active peptides on asymmetric bilayers that generate a net intramembrane potential. In particular, we posit that an electrophysiological approach for monitoring leaflet asymmetry and assessing alamethicin behavior should be considered.

To address this need, we demonstrate for the first time parallel, capacitance-based measurements [33,34,36,51] of intramembrane potential on arrays of asymmetric DIBs assembled in a microfluidic device to characterize the stability of leaflet asymmetry in the presence and absence of membrane-active peptides. Specifically, we used a revised version of our recent microfluidic DIB platform [52] that is now capable of generating a stream of alternating aqueous droplet compositions to assemble arrays of asymmetric DIBs. Asymmetric membranes are assembled from ester-linked DPhPC and ether-linked DOPhPC lipids, a choice that results in a non-zero transmembrane potential due to the higher relative dipole density of ester-linked lipids compared to ether-linked lipids [53]. Capacitance measurements are performed on eight DIBs in parallel via thin-film surface electrodes positioned beneath droplet pairs within the device. After verifying the ability to measure the transmembrane potential in DPhPC/DOPhPC DIBs, we monitored the transient stability and lifetime of leaflet asymmetry in the presence and absence of alamethicin (alm), a pore-forming peptide known to promote lipid "flip-flop" and scramble asymmetric membranes. We also performed cyclic voltammetry (CV) measurements to analyze the effects of asymmetry-induced dipole potential difference on the voltage-driven formation of ion channels by alm peptides.

2. Experimental section

2.1. Materials

Aqueous lipid solutions containing unilamellar liposomes are prepared with 2 mg/mL of 1,2-diphytanoyl-*sn*-glycero-3-phosphocholine (DPhPC, Avanti Polar Lipids) and 1,2-di-O-phytanoyl-*sn*-glycero-phosphocholine (DOPhPC, Avanti Polar Lipids) in 10 mM 3-(*N*-morpholino) propanesulfonic acid (MOPS, Sigma) buffer and 1 M sodium chloride (NaCl, Sigma). For each, the lyophilized powder is dissolved in aqueous buffer solution, followed by five freeze/thaw cycles. Then, the prepared stock solution is extruded through 100 nm pore polycarbonate membranes (NanoSizer extruders, T&T Scientific) to create a unilamellar liposome solution; this liposome solution is stored at 4 °C between experiments. Tetradecane (Sigma) is used as the organic solvent phase in all experiments. Tetradecane provides consistent ohmic contact between droplets and electrodes in the microfluidic device, whereas hexadecane results in a capacitive connection between droplets and electrodes.

Alamethicin peptide (A.G. Scientific) from the fungus *Trichoderma veride* is dissolved in ethanol (Sigma) at 2.5 mg/mL to create a stock solution that is stored at −20 °C. The stock solution is diluted twice serially, first to 25 μg/mL alamethicin and then to the desired final peptide concentration, using the 2 mg/mL liposome solution as the diluent.

2.2. Microfluidic device design, fabrication, and operation

The microfluidic device is designed to produce, route, and capture pairs of aqueous droplets dispersed in oil. Two directly-opposed T-junction droplet generators produce streams of droplets of alternating compositions. The droplet stream is routed downstream to an array of hydrodynamic traps where droplets are captured [52]. The device dimensions are tailored for a 125 μm diameter droplets. Each trap has a width of 240 μm and length of 130 μm, which is designed to hold two droplets, and two, narrow exit channels of 35 μm width and 20 μm length that serve to direct the droplets into vacant traps without allowing the droplets to escape after capture. The device has a uniform depth of 125 μm.

The microchips are fabricated using standard photo- and soft-lithography techniques. Briefly, a silicon wafer is spin-coated with photoresist and exposed to UV light through a chrome photomask using a photolithography aligner such that unmasked areas are cross-linked. Then, uncured photoresist is removed, followed by a deep reactive-ion etching process to etch the silicon wafer to a depth of 125 μm. After the master wafer is stripped of remaining polymerized photoresist and silanized to prevent adhesion during soft-lithography, uncured Sylgard 184 (Dow-Corning) PDMS (10:1 wt-wt ratio of base to curing agent) is

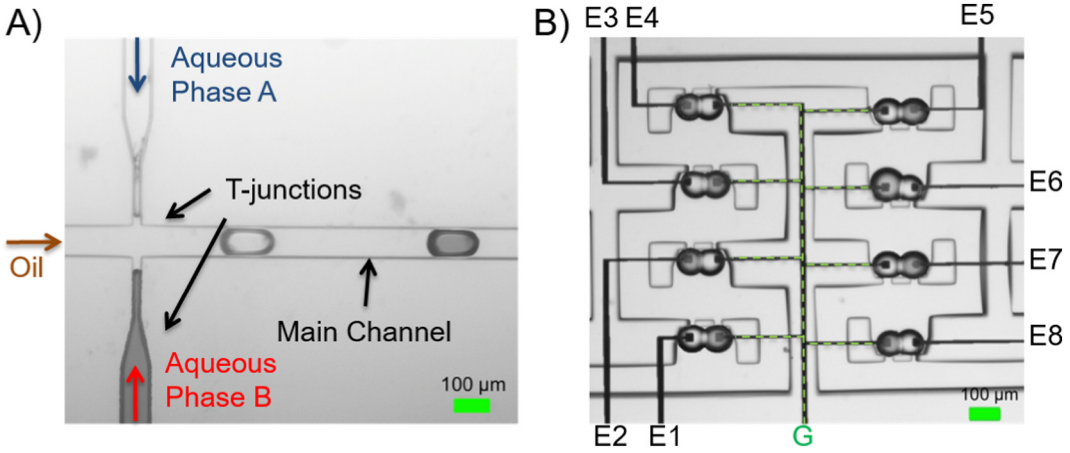

Fig. 1. A) 10× magnified image of the opposing T-junction droplet generators used to form droplets of alternating aqueous composition. Oil flow rate: 0.4–1.0 µL/min. Aqueous flow rate: 0.005–0.5 µL/min. B) 10× magnified image of the microfluidic droplet routing and trapping pathway used to form asymmetric DIBs, including square electrode pads deposited on the glass surface under each droplet trap. The central electrodes (green dashed line overlays) are connected and used as a common ground connection (G), while each black electrode (E1-E8) is connected to an independent channel of the 8-channel patch clamp amplifier headstage. (For interpretation of the references to color in this figure legend, the reader is referred to the web version of this article.)

poured over the wafer, degassed, and baked at 80 °C for a minimum of 2 h. Cured PDMS substrates are sliced and peeled from the master wafer. Inlet and outlet access holes are created using a 0.75 mm diameter biopsy punch. The PDMS substrate is then exposed to oxygen plasma and physically bonded to a glass slide containing thin-film electrodes. The sealed devices are baked at 80 °C for at least 48 h to create restore the hydrophobicity of the PDMS micro-channel walls.

Thin-film electrodes are placed strategically such that each pad is directly under the trapped droplet (Fig. 1B). Similar to the microfluidic fabrication, a chrome photomask with the desired electrode pattern is developed, followed by photolithography on a glass wafer (Borofloat). A single electrode pathway consists of a 30 × 30 µm square droplet pad with a variable-width (10-500µm) lead that extends to the edge of the wafer, where it terminates at a 3 × 3 mm square contact. A dual gun electron beam evaporation chamber is used to deposit a 10 nm adhesive layer of chrome and then 300 nm of silver onto the glass wafer. Next, lift-off in acetone and isopropyl alcohol is performed to remove unattached metals. Prior to bonding with PDMS micro-channels, bleach is pipetted onto the 30 × 30 µm electrode pads for 5 s to form silver-silver chloride reversible electrodes. Silver wire is soldered onto each 3 × 3 mm contact to connect to the patch clamp amplifier.

A dual syringe pump (Gemini 88, KD Scientific) is used to control the volumetric flow rates of the dispersed aqueous phases. Another syringe pump (Harvard Scientific) is used to control the flow rate of the continuous oil phase. PTFE tubing and 23-gauge blunt stainless-steel needles are used to connect syringes to inlet ports of the microfluidic device.

2.3. Electrical measurements and imaging

Voltage-induced currents across DIBs are monitored using an 8-channel patch clamp amplifier (Triton, Tecella LLC) and TecellaLab software that provides digital control of the applied voltage to each membrane. A triangular voltage waveform (typically 40 mV, 50 Hz) generated in TecellaLab is applied to each membrane to monitor bilayer capacitance. For cyclic voltammetry scans, the DC holding voltage is varied manually in an incremental, stepwise fashion to approximate increasing and decreasing linear voltage ramps (10 mV steps, 1 s step time, 10 mV/s effective scan rate). Our use of 1 M NaCl in the droplets serves to amplify the ionic current through alamethicin channels inserted during cyclic voltammetry measurements. Thus, we select a minimum conductance threshold of 100 µS/cm^2 for determining V*, appropriately higher than the 8 µS/cm^2 threshold used in prior experiments with 0.1 M NaCl [54, 55]. Measured currents are sampled at 2 kHz, filtered at 1 kHz using a built-in low-pass filter, and digitized using 16-bit A/D conversion within the Triton. Images of DIBs within the device are obtained using a CCD camera (QImaging QIClick) connected to an inverted microscope (Olympus IX51). Specific capacitance measurements were obtained using two suspended droplets and an Axopatch 200B patch clamp amplifier (Molecular Devices) as described previously [56,57].

3. Results

3.1. Rapid microfluidic assembly of DIBs between droplets of alternating composition

Asymmetric droplet interface bilayers were assembled using a modified version of our previously described microfluidic chip [52] that now features opposing T-junction inlets. First developed by Zheng, et al. [58], the opposing T-junctions production of a stream of alternating droplets from the two inlet channels, respectively, under specific flow conditions. Fig. 1A shows the opposing T-junctions in our device from which aqueous droplets with different compositions were sheared by a continuous flow of oil in the main channel. Alternating droplets were produced when the capillary number ranged from 0.002 to 0.04 and the water fraction of the aqueous inlets (per total liquid flow rate) was maintained between 0.4 and 0.8 [58]. Volumetric flow rates for the oil and water that satisfy these criteria are provided in the caption of Fig. 1. Under these conditions droplets were created, routed, and captured in pairs using channel and droplet trap geometries and dimensions selected based on a hydrodynamic resistance model used to predict flow rate and pressure distribution within the chip [52]. After two droplets arrived in a trap, a DIB formed spontaneously within a few seconds. The image in Fig. 1B shows eight DIBs, each with symmetric DPhPC leaflets but dissimilar aqueous compositions containing either buffer (lighter droplets in the figure) or buffer with water-soluble dye (darker droplets). This approach was then applied to assemble and characterize DIBs consisting of one DPhPC leaflet and one DOPhPC leaflet.

3.2. On-chip electrodes enable quantitative assessment of bilayer leaflet asymmetry

We previously demonstrated simultaneous electrical interrogation of multiple DIBs formed in a microfluidic chip featuring thin-film Ag/AgCl electrodes residing underneath the droplet pairs [52]. In the

present study, we leveraged this same capability to perform capacitance-based measurements of transmembrane potential caused by leaflet asymmetry in DIBs. This technique is based on the known voltage dependence of bilayer capacitance, C, which can be described by: [33–36, 51, 59]

$$C(V_c, \Delta\Psi) = C_0(1 + \alpha(V_c + \Delta\Psi)^2) \quad (1)$$

Here, V_c is the clamping potential applied by a patch-clamp amplifier (or analogous device), $\Delta\Psi$ is the transmembrane potential difference due to lipid leaflet asymmetry, C_0 is the membrane capacitance when $V_c = -\Delta\Psi$, and α is the capacitive electrowetting constant. The total potential difference across a membrane is the sum of V_c and $\Delta\Psi$. Differences in both lipid surface potential, $\Delta\Psi_S$, and lipid dipole potential, $\Delta\Psi_D$, contribute to the transmembrane potential difference due to leaflet asymmetry [34], as given by:

$$\Delta\Psi = \Delta\Psi_S + \Delta\Psi_D \quad (2)$$

$\Delta\Psi$ can also arise from composition differences (e.g. salt concentration) in the aqueous media on opposite sides of the membrane that affect the net surface charge or dipole potential (e.g. incorporation of membrane-absorbing dipoles). Thus, Eq. (1) indicates that the transmembrane potential difference established by leaflet asymmetry can be determined by measuring capacitance as a function of voltage to identify the value of V_c that fully negates $\Delta\Psi$ and thereby minimizes capacitance. Measurements of $C(V_c)$ also enable calculation of C_0 and α values from Eq. (1) (refer to supporting information (SI) for additional details).

Independent, multi-channel electrical measurements were made using a Tecella Triton 8-channel patch clamp amplifier. The DIBs were independently accessed via 8 measurement channels (electrodes marked E1 through E8 in Fig. 1B) and a common ground (G) on the Triton amplifier. Note in Fig. 1B that routing a stream of alternating droplet compositions into our electrode trap array resulted in alternating droplet compositions on the measurement and ground electrodes for successive DIBs. To describe the compositions of each leaflet in an asymmetric DIB and define the applied electrical condition of each droplet, we denote a droplet residing on a measurement electrode (E) and its corresponding lipid monolayer as the *cis* side of the membrane, while the adjoined droplet on the grounded electrode (G) and its surrounding monolayer represent the *trans* side of the bilayer. In shorthand form, leaflet compositions of each DIB are written as *cis/trans* (e.g. DPhPC/DOPC = *cis* (E) / *trans* (G)).

Leaflet asymmetry in a DIB was confirmed via electrical measurements of AC capacitive currents obtained while performing a step-wise DC voltage sweep required to elucidate the electrowetting response. This procedure is illustrated in Fig. 2. Eq. (1) describes the relationship between membrane capacitance and both the clamping voltage and transmembrane potential that arises due to asymmetric leaflet compositions. The asymmetry imposed by an ester-linked DPhPC leaflet and an ether-linked DOPhPC leaflet has been reported to generate a net $\Delta\Psi_D$ of 135 mV [49], with the DPhPC leaflet carrying the more positive nominal dipole potential. The choice of phosphatidylcholine headgroups, as well as the use of identical buffer solutions on each side of the membrane minimized the possibility of differences in surface potential across the membrane; thus, it was assumed that $\Delta\Psi_S = 0$ mV for the experiments reported herein. Fig. 2A shows the predicted potential profiles across a DPhPC/DOPhPC membrane with $V_c = 0$ mV (left) and $V_c = -\Delta\Psi_D$ (right). In the latter case, clamping the applied potential at a value equal in magnitude but opposite in sign to $\Delta\Psi_D$ zeroes the transmembrane potential.

Fig. 2B and C, respectively, show the applied voltage waveform and resulting current used to compute capacitance-voltage (C-V) curves. The input voltage waveform (see inset) consisted of an AC triangle wave overlaid on a variable DC bias. This composite signal elicited a capacitive square-wave current (Fig. 2C and insets in 2D) from the AC component, while invoking electrowetting described by Eq. (1) from the DC bias (varied in 12.5 mV increments every 30 s). Nominal capacitance is computed from the amplitude of the square waveform current, I_{sw}, at the end of each voltage step and the amplitude, A, and frequency, f, of the triangle AC voltage via $C = I_{SW}/(4Af)$. The "hourglass" shape of the total current response in Fig. 2C visually confirms the quadratic dependence of C on voltage, where increases in capacitance can be caused by both electrowetting-induced area growth and electrocompressive reductions in thickness. Fig. 2E shows representative C-V curves obtained from a DPhPC/DOPhPC DIB, a DOPhPC/DPhPC DIB, and a symmetric DPhPC DIB. As stated by Eq. (1), capacitance reaches a minimum when $V_c = -\Delta\Psi_D$, where the net transmembrane potential is zero (refer to SI for details of $\Delta\Psi_D$ determination). The quadratic C-V curve for a DPhPC/DOPhPC bilayer is shifted towards negative voltage by an amount equal to $|\Delta\Psi_D|$. Similarly, the C-V curve for a DOPhPC/DPhPC bilayer is shifted by $|\Delta\Psi_D|$ in the positive direction, whereas symmetric DIBs display minimum nominal capacitance at $V_c = 0$. Specific capacitance, or C_M, is an intrinsic property that scales inversely with membrane hydrophobic region thickness. Separate testing with two-droplet symmetric and asymmetric DIBs confirmed that the voltage dependence of bilayer specific capacitance is affected by the net dipole potential difference; i.e. minimum C_M is observed when $V_c + \Delta\Psi_D = 0$. Stated differently, membrane thickness increases as V_c approaches $-\Delta\Psi_D$ (refer to Fig. S2 in SI for C_M values and comparisons).

Measurements of 8 DIBs formed from alternating DPhPC and DOPhPC droplets within our microfluidic device included 4 DIBs with DPhPC droplets on measurement electrodes and 4 DIBs with DPhPC droplets on ground electrodes, resulting in minimum capacitance occurring at opposite potentials. Fig. 3A shows C-V scans obtained from electrowetting measurements made with a set of 8 separate, asymmetric DIBs without alm formed in the microfluidic chip at time, $t = 0$. This set yielded 8 separate values of $\Delta\Psi_D$, with average and standard deviation of 136.6 ± 0.6 mV for $|\Delta\Psi_D|$. Across 12 DPhPC/DOPhPC (*cis/trans*) bilayers assembled in three separate trials (i.e. half of the 3 sets of 8 DIBs) with the microfluidic chip, calculated $\Delta\Psi_D$ values were c.a. +137 ± 0.9 mV which compares well with the +135 mV value determined by mechanoelectrical measurements of DPhPC/DOPhPC DIBs [49]. In both our experiments and those of Freeman et al. [49], reversing the asymmetry to DOPhPC/DPhPC simply resulted in a change in the polarity of the measured $\Delta\Psi_D$ (−137 ± 1.0 mV, see Fig. 2E). Measured $\Delta\Psi_D$ values were ~0 mV in the case of symmetric DPhPC (Fig. 2E) and DOPhPC (not shown) DIBs. For comparison, a separate measurement was performed on a DIB containing symmetric acyl chains and asymmetric lipid headgroup charge. The measured C-V curve of a DPhPG/DPhPC DIB (SI Fig. S4) shows that it generates a net potential of −93 mV due to the unbalanced distribution of negative PG lipids. Thus, the methodology described above can be used to study transmembrane potentials arising from both asymmetric distributions of acyl chains and headgroups.

3.3. Quantitatively tracking membrane asymmetry over time

Next, experiments were performed to explore the temporal stability of leaflet asymmetry in DPhPC/DOPhPC DIBs assembled in the presence and absence of alm peptides. Fig. 3B shows representative C-V traces obtained at $t = 0$, 5, and 10 h from a single DPhPC/DOPhPC bilayer without alamethicin. For comparison, Fig. 4A shows representative C-V traces obtained at similar time intervals with an asymmetric DPhPC/DOPhPC DIB containing 2 μM alm in the *cis* (DPhPC) droplet. At time $t = 0$, the presence of alm does not affect the |137 mV| intramembrane potential that stems from leaflet asymmetry. The C-V curves in Fig. 4A shift towards 0 mV with increasing elapsed time, whereas the curves in Fig. 3B do not shift with time. The C-V curves obtained at each time interval were used to calculate average values of $\Delta\Psi_D$ as a function of time which are shown in Fig. 4B. The dipole potential difference across peptide-free DPhPC/DOPhPC

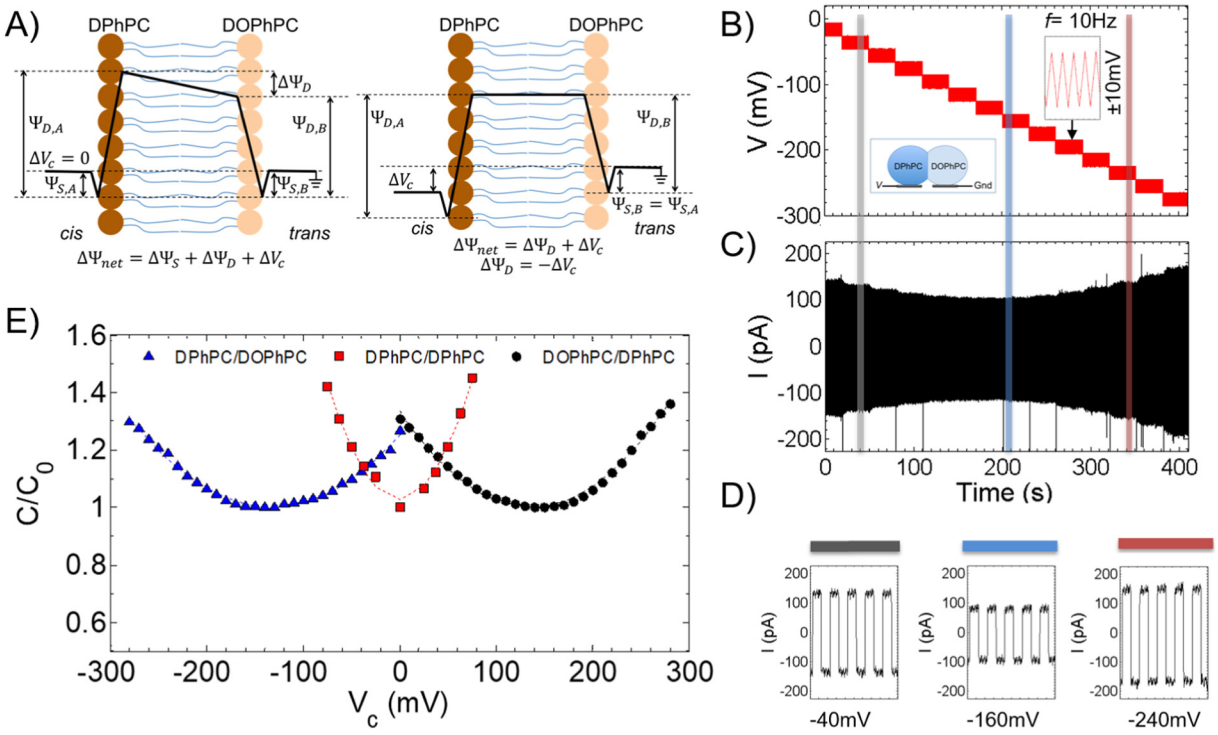

Fig. 2. A) Illustration of membrane potential profiles, including the difference in dipole potential ($\Delta\Psi_D$) of DPhPC and DOPhPC leaflets forming an asymmetric DIB. B) Applied voltage signal and (C) the resulting current measured during an electrowetting experiment to measure asymmetric membrane potential in a DPhPC/DOPhPC DIB. 30 s steps in DC voltage were applied on top of a continuous high frequency triangle wave used to elicit capacitive square-wave current. D) Insets show 500 ms of capacitive current corresponding to the colored stripes in (C). E) Normalized capacitance as a function of clamped voltage, V_c, was shifted by the intramembrane potential difference that existed with asymmetric DPhPC/DOPhPC or DOPhPC/DPhPC DIBs. Symmetric DIBs produced C/C_0 curves centered at $V_c = 0$ mV.

membranes is stable for > 8 h (experiments to date extend to 18 h at which point no change in $\Delta\Psi_D$ was observed), but the presence of alm causes a gradual reduction in the magnitude of $\Delta\Psi_D$. In asymmetric DIBs including 1 μM alm on the DPhPC (*cis*) leaflet, $\Delta\Psi_D$ decreased by 27 mV, from +137 mV to +110 mV, within 4 h of the initial bilayer formation. With a lower peptide concentration of 0.5 μM included in the *cis* droplet, $\Delta\Psi_D$ decreased to only +115 mV within the first 4 h of bilayer formation. Data in Fig. 4B thus suggests that the rate of decay in $\Delta\Psi_D$ is positively correlated with the concentration of surface-bound alm peptides.

Alamethicin is known to insert into the bilayer and form transmembrane pores from the *cis* side (convention as defined above, *trans* grounded) with either sufficiently high peptide concentration or positive voltage [60–62]. Therefore, because our approach to assess $\Delta\Psi_D$ requires measuring capacitive current at positive and negative DC voltage steps, pore-forming alm peptides were added: (a) at sufficiently low concentrations; and (b) to only DPhPC-containing droplets, to prevent increases in current due to alm pore formation while executing the DC voltage sweep needed to minimize capacitance (see example in Fig. 2B). Alm concentrations of 0.5 μM and 1 μM with 2.4 mM liposomes correspond to peptide/lipid (P/L) ratios of ~1/4800 and 1/2400, respectively. These ratios are an order of magnitude lower than the P/L ratio (~1/100 for DPhPC) at which alm spontaneously inserts without an applied voltage [61]. Thus, for the low P/L ratios used herein, alm peptides are assumed to be in an uninserted, surface-bound state [62] when the applied potential is below the threshold insertion voltage. In the surface-bound state, helical alamethicin peptide monomers orient parallel to the plane of the membrane to associate closely with the lipid headgroups of the *cis* DPhPC leaflet of the asymmetric DIB (as well as the outer leaflet headgroups of excess liposomes in the *cis* droplet).

3.4. Characterizing the effect of asymmetry on voltage-driven alamethicin insertion

Having shown that dipole potential reduces by nearly 20% over the course of 5 h in DPhPC/DOPhPC membranes (Fig. 4B), a series of cyclic voltammetry (CV) measurements were performed to explore converse effects of a non-zero intramembrane dipole potential on the threshold

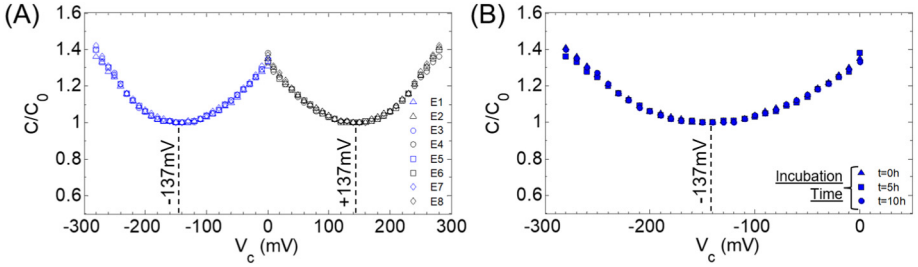

Fig. 3. A) Capacitance, plotted as C/C_{min}, for 8 separate asymmetric DIBs formed in the microfluidic chip at time $t = 0$. Four of the DIBs were DPhPC/DOPhPC (*cis/trans)* while the other four were DOPhPC/DPhPC. B) Voltage-dependent capacitance measured over several hours for an asymmetric DPhPC/DOPhPC DIB.

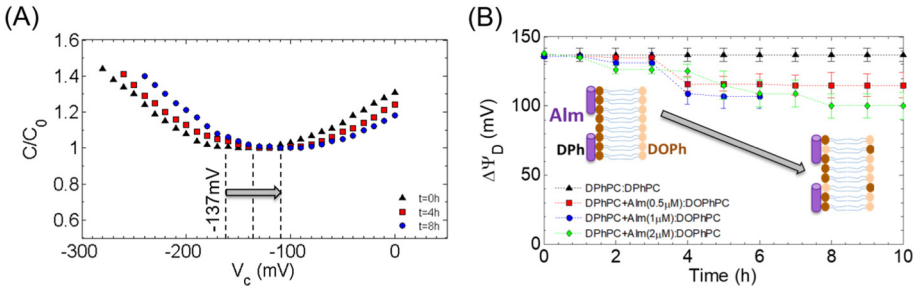

Fig. 4. A) Voltage-dependent capacitance measured at various time points over 8 h with an asymmetric DPhPC/DOPhPC DIB incorporating 2 μM alamethicin peptide in the *cis* droplet. B) Measured values for $\Delta\Psi_D$ (average ± std. dev.) as a function of time, including results from experiments shown in Figs. 3B and 4A.

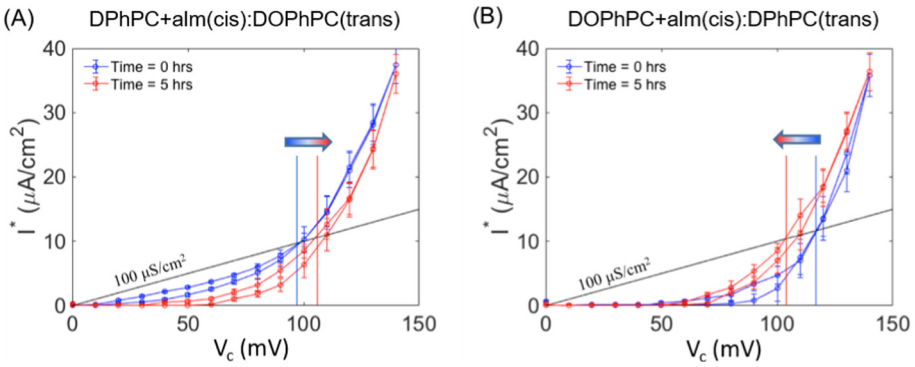

Fig. 5. Cyclic voltammetry curves obtained upon initial formation and after 5 h of incubation with asymmetric DPhPC/DOPhPC DIBs incorporating alamethicin in one droplet. The current response is normalized by membrane area for each scan and plotted versus the applied voltage. Normalized current for asymmetric DIB of (A) DPhPC + alm:DOPhPC and (B) DOPhPC + alm:DPhPC. The black line represents the specific conductance threshold (100 μS/cm^2) used to determine the voltage threshold for alamethicin insertion.

voltage (V^*) required to drive alm insertion and ion channel formation. V^* is a thermodynamic parameter dependent on peptide concentration, temperature, and membrane properties [54,55,63]. CV scans were performed immediately after forming bilayers ($t = 0$) in the presence of alm and again after 5 h of incubation with alm in the surface-bound state. Fig. 5A–B show averaged current per unit membrane area versus voltage (I^*-V) curves obtained from CV experiments with DPhPC/DOPhPC and DOPhPC/DPhPC DIBs containing 1 μM alm in the *cis* droplets. V^* is determined as the voltage at which specific conductance increases above an arbitrary threshold of 100 μS/cm^2 (shown as a thin, solid line in each plot). Fig. 5A shows that V^* increases during the 5-hour incubation period (from +99 mV to +110 mV) with alm added to the DPhPC side of *a* DPhPC/DOPhPC membrane. In contrast, V^* decreases (+113 mV to +105 mV) during the incubation period with alm added to the *cis* side of a DOPhPC/DPhPC membrane (see arrow in Fig. 5B).

4. Discussion

Our results demonstrate that the benefits of the multi-phase DIB system for prescribing compositional leaflet asymmetry and a microfluidic array with embedded electrodes for rapid assembly and simultaneous electrophysiology of multiple bilayers can be married to study lipid translocation. To our knowledge, this is the first report in which lipid flip-flop has been quantified in DIBs. Leveraging the ability to electrically probe each bilayer in the array, we specifically chose to employ a capacitance-based measurement method, in addition to cyclic voltammetry, for tracking asymmetry. With this in mind, it is helpful to frame what is known about lipid flip-flop in a bilayer that could contain residual oil and the applicability of our approach for studying flip-flop in model membranes containing other lipids and peptides.

The main mechanism opposing lipid flip-flop is the hydrophobic effect, which establishes an energetic barrier that discourages polar headgroups from crossing the central hydrocarbon region of the membrane [64]. In the case of experiments with DIBs (or even BLMs), assembled from lipids organized at interfaces between water and organic solvent (oil), residual oil the bilayer region can alter this energy landscape. For example, oil retention in the bilayer is known to increase the hydrophobic thickness of the membrane, and we have measured previously that it can also alter membrane tension by disrupting lipid packing [56]. While the first effect should correlate to a higher energy barrier for transleaflet flip-flop, solvents that perturb the lateral packing of lipids enough to promote defects in the membrane could actually increase the likelihood of flip-flop. To our knowledge these effects have not been extensively quantified in prior reports. Nonetheless, in this study oil-induced defects that aid flip-flop are not expected, since it is known that tetradecane (C14) and longer alkane oils do not interdigitate among the lipid acyl chains and, thus, do not alter their packing [65, 66].

The archaeal lipid DPhPC is one of the most popular lipids for BLM and DIB experiments [55], despite it not being found in eukaryotic or prokaryotic membranes. The isoprenoid acyl chains yield bilayers exhibiting high stability and membrane impermeability. Given that DOPhPC shares identical isoprenoid acyl chains, it is not surprising that DOPhPC lipids also yield highly-resistive bilayers at the interface between droplets. However, lipids that better represent the headgroup and acyl chain compositions of eukaryotic and prokaryotic systems can also be used to form DIBs [67]. Therefore, the DIB technique described herein is accessible for use studying lipid flip-flop and the effects of peptides or other small molecules on flip-flop in membranes displaying a wide variety of compositional asymmetries. For example, the techniques used herein to study alm-induced scrambling could be applied to investigate reported flop-rate increases caused by WALP or KALP peptides [15, 16]. We also showed that the technique can be used to quantify transmembrane potentials generated by lipid headgroup charge asymmetries.

4.1. Surface-bound alamethicin promotes lipid flip-flop and scrambles leaflet asymmetry

Alm binding to membranes consists first of a transition from a purely solvated, monomeric state in bulk water to a surface-bound "S" state in which peptide monomers on a lipid leaflet orient parallel to the membrane [68]. With sufficient increase in peptide concentration or

applied transmembrane potential, monomers transition from the "S" state to an inserted "I" state in which the peptide monomers orient perpendicular to the plane of the membrane. "I" state monomers then associate and dissociate rapidly, forming transient conductive oligomeric pores or channels. Given this understanding, we expect that alm may exist in the "S" state anywhere across the lipid monolayers formed at the oil/water interfaces of droplets used to form DIBs. However, alm peptides are only expected to transition to the "I" state in regions of leaflets comprising the bilayer area between droplets. Further, alm partitioning into the hydrocarbon phase of bulk solvent surrounding droplets is assumed to be negligible due to its amphiphilic structure.

Collectively, the data presented in Fig. 4 and Fig. 5 indicate that surface-bound alamethicin monomers reduce the difference in dipole potential across asymmetric DPhPC/DOPhPC membranes over time via lipid translocation or "flip-flop". In the absence of alm, the stability of $\Delta\Psi_D$ values for DPhPC/DOPhPC membranes (Fig. 3B, D) shows that leaflet compositions are maintained for many hours, a result that is consistent with prior reports of extremely low rates of lipid flip-flop in defect free lipid membranes [13]. The steady dipole potential difference in alm-free DPhPC/DOPhPC bilayers also confirms that lipid exchange between monolayers via diffusion through the oil phase is negligible. In contrast, we observe $\Delta\Psi_D$ to slowly decrease, from +136 mV to +116 mV or lower over the course of 5 h, when alm is bound to the surface of one membrane leaflet. The alm-associated decrease in $\Delta\Psi_D$ is specifically attributed to peptide-induced flip-flop, as others have observed in asymmetric vesicles and planar lipid bilayers [69–71]. The fact that the magnitude of change in intramembrane potential was also affected by the amount of peptide present further identifies alamethicin as a catalyst for the change in dipole potential. We also considered the possibility of alamethicin peptide directly affecting monolayer dipole densities; the peptide monomer has a dipole moment of 65 mD [72, 73]. However, the inclusion of alamethicin on only one side of the membrane did not induce any measurable change in the magnitude $\Delta\Psi_D$ (Fig. 4) at $t = 0$. It is also known that membrane-bound alamethicin exists in dynamic thermodynamic equilibrium with the lipids and peptides in solution, and the binding and distribution of alm peptide responds quickly (i.e. within seconds) when titrating peptides into liposomes or vice versa [74–76]. As such, the slow changes measured in V^* over the course of 5 h (Fig. 5A,B) point to gradual changes in the lipid distribution in the membrane.

It is also possible that alamethicin translocates through the hydrophobic core of the membrane to the opposite lipid leaflet. In fact, Hall demonstrated this behavior when maintaining an applied voltage above V^* across asymmetric planar bilayers [50]. However, given the direct correlation between peptide concentration and V^* (i.e. V^* increases as concentration decreases) [55], this outcome would be expected to increase V^* in all cases where alm is incorporated into the *cis* droplet alone. Translocation of peptide from the *cis* droplet to the *trans* droplet would reduce the *cis* droplet peptide concentration and increase V^*. We only observe a gradual V^* increase in the DPhPC + alm/DOPhPC case (Fig. 5). We have further examined the possibility of peptide translocation by applying negative voltages of |200–300 mV| after the 5-hour incubation period shown in Fig. 5, but we saw no signs of peptide insertion and channel formation from the *trans* droplet (data not shown). Ruling out peptide translocation rules out the possibility of decreasing peptide concentration in the *cis* compartment, as well as any effects associated with the peptide dipole moment affecting the *trans* leaflet. We thus attribute the measured decreases in intramembrane potential versus time for asymmetric membranes to lipid translocation. It is important to note that alamethicin peptides promote an increase in the rate of flip-flop even in the surface-bound state (i.e. when there is no voltage applied to drive channel formation). From the data in Fig. 4B we estimated the half-life of the asymmetry as it relates to the kinetics of lipid flip-flop to be around 15 h (peptide/lipid ratio of 1/2500; refer to Fig. S5 in SI). While alamethicin insertion is sensitive to several factors, including lipid type, salt concentration, and temperature, our data for asymmetric DPhPC/DOPhPC membranes suggest: (a) the gradual changes in V^* for alm insertion are attributed primarily to changing leaflet compositions and subsequent changes in membrane fluidity or packing as lipids translocate; and (b) corresponding changes in $\Delta\Psi_D$ contribute only weakly to the voltage-dependent alamethicin insertion.

4.2. Intramembrane $\Delta\Psi_D$ minimally affects voltage-dependent behavior of alamethicin

A priori, we questioned whether the value of V^* for alamethicin insertion would be shifted by the full magnitude of $\Delta\Psi_D$ that is induced by asymmetric leaflets and which alters the voltage-dependent electrowetting response (i.e. Fig. 2E). Therefore, we performed I^*-V sweeps on asymmetric and symmetric bilayers containing alamethicin to quantify the effect of the non-zero intramembrane potential on the threshold voltage required to insert alm peptides. For both asymmetric membranes (Fig. 5A, B) and symmetric DPhPC membranes (Fig. S6), the measured current remained near zero until the transmembrane clamping voltage exceeded V^*. Once the voltage exceeded the threshold, current increased exponentially as the membrane became populated by peptide-stabilized pores. Visual inspection of I^*-V curves from asymmetric membranes revealed that $|\Delta\Psi_D|$ did not shift V^* by its full value of 137 mV: alamethicin insertion occurred at a value of V^* between 100 and 125 mV for all cases tested herein. Values obtained for V^* are provided for each case of lipid symmetry (illustrated in Fig. 6A) in Table 1 and graphed in Fig. 6B. Moreover, we found that V^* for a symmetric DPhPC bilayer was not statistically different from that of symmetric DOPhPC membrane or an asymmetric bilayer with alm added to the DOPhC leaflet. Our data do show that V^* was statistically lower when alm was added to the DPhPC leaflet of an asymmetric membrane, however. This result is consistent with the idea that less voltage (energy) is required to insert alm into a leaflet at higher dipole potential (i.e. in the direction of the electric field induced by $\Delta\Psi_D$) [50].

The data in Table 1 and Fig. 6 clearly show that V^* is not altered by the full magnitude of $\Delta\Psi_D$ associated with asymmetric DPhPC/DOPhPC leaflets. These findings are presented as evidence that the non-zero

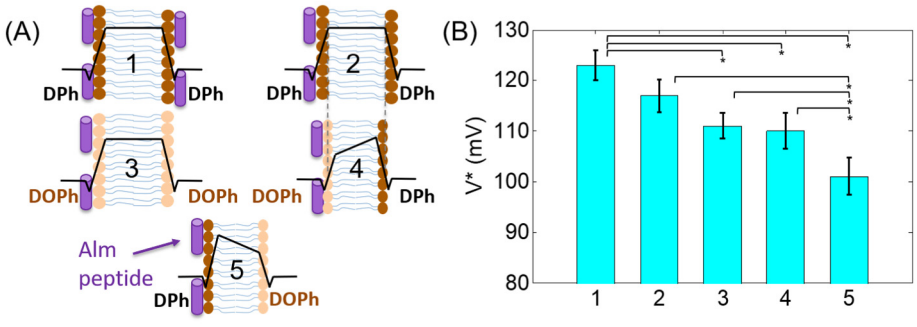

Fig. 6. A) Illustration of leaflet lipid compositions and location of alamethicin for the five cases listed in Table 1. Case 1 represents symmetric DPhPC/DPhPC (*cis* left, *trans* grounded right) with 1 μM alamethicin included on both sides of the membrane. Prior to applying external voltages, alamethicin peptide monomers are in the surface-bound state at the chosen peptide/lipid ratio (P/L ~1/2000). All other cases include 1 μM only on the *cis* droplet. B) Graph showing average V^* values (error bars show ± std. dev) measured with the varying cases of DPhPC/DOPhPC asymmetry shown in (A). The graph aides in visualizing trends with numerical values from Table 1. Horizontal brackets with asterisks indicate comparisons of groups whose averages are statistically different ($p < 0.05$).

Table 1
Voltage thresholds (V^*, ΔV^*) for alamethicin insertion.

	DIB composition	V^* (mV)	ΔV^* (mV)
1	DPhPC + alm:DPhPC + alm	123 ± 3.0 (n = 4)	0
2	DPhPC + alm:DPhPC	117 ± 3.2 (n = 4)	−6
3	DOPhPC + alm: DOPhPC	111 ± 2.5 (n = 4)	−12
4	DOPhPC + alm: DPhPC	110 ± 3.5 (n = 4)	−13
5	DPhPC + alm: DOPhPC	101 ± 3.6 (n = 4)	−22

'alm' = alamethicin concentration of 1 μM in the droplet.

$|\Delta\Psi_D|$ of 137 mV imposed by ester-ether lipid leaflet asymmetry both i) is insufficient to promote alm insertion by itself and ii) does not simply add to the clamping potential value to determine V^*. The weak dependence of alm insertion on the dipole potential may indicate that, at the molecular level, surface-bound peptides associated with lipid headgroups are positioned outside (or partially outside) of the electric field generated by opposing leaflet dipole potentials (Fig. 6A). As a result, the peptides require some additional clamping potential to overcome the energy-barrier for insertion.

5. Conclusions

By incorporating different lipid types into separate droplets, the droplet interface bilayer method offers facile assembly of lipid bilayers with asymmetric leaflet compositions. In this work, we leveraged a microfluidic system capable of generating streams of alternating droplet composition to assemble arrays of lipid bilayers with asymmetric leaflet compositions. This device employs a scalable droplet trapping scheme for efficient DIB formation between distinct pairs of lipid-coated droplets and features integrated thin-film electrodes that enable electrophysiology of multiple bilayers in the array at once. With these capabilities, we assembled asymmetric leaflet bilayers between DPhPC-coated and DOPhPC-coated droplets, and we employed capacitance-based intramembrane potential measurements to quantify lipid asymmetry in the presence and absence of membrane-active alamethicin peptides. Our parallel measurements of sets of 8 asymmetric DIBs show that DPhPC/DOPhPC membranes exhibit an average intramembrane dipole potential difference of |137 mV|, which agrees well with values obtained by other means. Long-term measurements of the dipole potential difference show that lipid asymmetry is stable for at least 18 h in DPhPC/DOPhPC DIBs in the absence of membrane-active peptides. In contrast, the inclusion of surface-bound alamethicin peptides causes a gradual decrease in the |137 mV| dipole potential difference which is measured at time $t = 0$. These results allow us to conclude that surface-bound alamethicin facilitates the translocation and mixing of lipids across leaflets, which results in a lower magnitude dipole potential difference. This redistribution of lipids also affects the energy-barrier for alamethicin ion channel formation; we observed the threshold voltage required to drive alamethicin insertion increased over time when alamethicin was added to the DPhPC leaflet. The opposite trend was observed when alamethicin was surface-adsorbed to the DOPhPC leaflet. In addition, cyclic voltammetry revealed that alamethicin insertion is not significantly affected by the nominal intramembrane voltage created with DPhPC/DOPhPC and DOPhPC/DPhPC membranes, a finding that suggests surface-bound alamethicin peptides do not feel the portion of the total transmembrane electric field exerted by an internal dipole potential difference between leaflets. If true, one might suspect that a surface potential difference caused by headgroup asymmetry across leaflets may exert a greater effect on the nominal value of threshold voltage.

Author contribution statement

Graham Taylor: Conceptualization, Methodology, Software, Formal Analysis, Investigation, Writing – Original Draft preparation, Visualization. **Mary-Anne Nguyen**: Conceptualization, Methodology, Software, Investigation, Writing – Original Draft preparation. **Subhadeep Koner**: Formal Analysis, Investigation. **Eric Freeman**: Conceptualization, Methodology. **C. Patrick Collier**: Conceptualization, Supervision, Funding Acquisition. **Stephen A Sarles**: Writing – Reviewing and Editing, Supervision, Funding Acquisition.

Transparency document

The Transparency document associated this article can be found, in online version.

Acknowledgments

The authors would like to acknowledge funding from the Air Force Office of Scientific Research Basic Research Initiative Grant number FA9550-12-1-0464. Microfluidic device fabrication and surface electrode patterning was conducted at the Center for Nanophase Materials Sciences, which is a DOE Office of Science User Facility. Also, the authors would like to acknowledge Dr. Yoke Tanaka at Tecella, LLC for assistance in configuring the Triton amplifier for multi-channel measurements.

Conflict of interest

GT works for T&T Scientific Corporation, a company that manufactures equipment used in the extrusion and production of liposomes.

Appendix A. Supplementary data

Supplementary data to this article can be found online at https://doi.org/10.1016/j.bbamem.2018.07.001.

References

[1] D.L. Daleke, Regulation of transbilayer plasma membrane phospholipid asymmetry, J. Lipid Res. 44 (2003) 233–242.
[2] G. van Meer, Dynamic transbilayer lipid asymmetry, Cold Spring Harb. Perspect. Biol. 3 (2011) a004671.
[3] D. Marquardt, B. Geier, G. Pabst, Asymmetric lipid membranes: towards more realistic model systems, Membranes 5 (2015) 180.
[4] T. Utsugi, A.J. Schroit, J. Connor, C.D. Bucana, I.J. Fidler, Elevated expression of phosphatidylserine in the outer membrane leaflet of human tumor cells and recognition by activated human blood monocytes, Cancer Res. 51 (1991) 3062–3066.
[5] R.A. Schlegel, P. Williamson, Phosphatidylserine, a death knell, Cell Death Differ. 8 (2001) 551.
[6] S. Pautot, B.J. Frisken, D.A. Weitz, Engineering asymmetric vesicles, Proc. Natl. Acad. Sci. 100 (2003) 10718–10721.
[7] S. Pautot, B.J. Frisken, D.A. Weitz, Production of unilamellar vesicles using an inverted emulsion, Langmuir 19 (2003) 2870–2879.
[8] J.C. Stachowiak, D.L. Richmond, T.H. Li, F. Brochard-Wyart, D.A. Fletcher, Inkjet formation of unilamellar lipid vesicles for cell-like encapsulation, Lab Chip 9 (2009) 2003–2009.
[9] K. Funakoshi, H. Suzuki, S. Takeuchi, Formation of giant lipid vesiclelike compartments from a planar lipid membrane by a pulsed jet flow, J. Am. Chem. Soc. 129 (2007) 12608–12609.
[10] J.C. Stachowiak, D.L. Richmond, T.H. Li, A.P. Liu, S.H. Parekh, D.A. Fletcher, Unilamellar vesicle formation and encapsulation by microfluidic jetting, Proc. Natl. Acad. Sci. 105 (2008) 4697–4702.
[11] D.L. Richmond, E.M. Schmid, S. Martens, J.C. Stachowiak, N. Liska, D.A. Fletcher, Forming giant vesicles with controlled membrane composition, asymmetry, and contents, Proc. Natl. Acad. Sci. 108 (2011) 9431.
[12] Q. Lin, E. London, Preparation of artificial plasma membrane mimicking vesicles with lipid asymmetry, PLoS One 9 (2014) e87903.
[13] D. Marquardt, F.A. Heberle, T. Miti, B. Eicher, E. London, J. Katsaras, G. Pabst, 1H NMR Shows Slow Phospholipid Flip-Flop in Gel and Fluid Bilayers, Langmuir 33 (15) (2017) 3731–3741.
[14] M. Garten, L.D. Mosgaard, T. Bornschlögl, S. Dieudonné, P. Bassereau, G.E.S. Toombes, Whole-GUV patch-clamping, Proc. Natl. Acad. Sci. 114 (2017) 328.
[15] M.A. Kol, A. van Dalen, A.I.P.M. de Kroon, B. de Kruijff, Translocation of phospholipids is facilitated by a subset of membrane-spanning proteins of the bacterial cytoplasmic membrane, J. Biol. Chem. 278 (2003) 24586–24593.
[16] M.A. Kol, A.N.C. van Laak, D.T.S. Rijkers, J.A. Killian, A.I.P.M. de Kroon, B. de Kruijff, Phospholipid flop induced by transmembrane peptides in model membranes

is modulated by lipid composition, Biochemistry 42 (2003) 231–237.
[17] S. Qian, W.T. Heller, Peptide-induced asymmetric distribution of charged lipids in a vesicle bilayer revealed by small-angle neutron scattering, J. Phys. Chem. B 115 (2011) 9831–9837.
[18] J.M. Crane, V. Kiessling, L.K. Tamm, Measuring lipid asymmetry in planar supported bilayers by fluorescence interference contrast microscopy, Langmuir 21 (2005) 1377–1388.
[19] W.-C. Lin, C.D. Blanchette, T.V. Ratto, M.L. Longo, Lipid asymmetry in DLPC/DSPC-supported lipid bilayers: a combined AFM and fluorescence microscopy study, Biophys. J. 90 (2006) 228–237.
[20] F.F. Rossetti, M. Textor, I. Reviakine, Asymmetric distribution of phosphatidyl serine in supported phospholipid bilayers on titanium dioxide, Langmuir 22 (2006) 3467–3473.
[21] V. Kiessling, J.M. Crane, L.K. Tamm, Transbilayer effects of raft-like lipid domains in asymmetric planar bilayers measured by single molecule tracking, Biophys. J. 91 (2006) 3313–3326.
[22] C. Wan, V. Kiessling, L.K. Tamm, Coupling of cholesterol-rich lipid phases in asymmetric bilayers, Biochemistry 47 (2008) 2190–2198.
[23] V. Kiessling, C. Wan, L.K. Tamm, Domain coupling in asymmetric lipid bilayers, Biochim. Biophys. Acta 1788 (2009) 64–71.
[24] R.M. Fabre, D.R. Talham, Stable supported lipid bilayers on zirconium phosphonate surfaces, Langmuir 25 (2009) 12644–12652.
[25] H.P. Wacklin, Composition and asymmetry in supported membranes formed by vesicle fusion, Langmuir 27 (2011) 7698–7707.
[26] S. Stanglmaier, S. Hertrich, K. Fritz, J.F. Moulin, M. Haese-Seiller, J.O. Rädler, B. Nickel, Asymmetric distribution of anionic phospholipids in supported lipid bilayers, Langmuir 28 (2012) 10818–10821.
[27] Noor F. Hussain, Amanda P. Siegel, Y. Ge, R. Jordan, Christoph A. Naumann, Bilayer asymmetry influences integrin sequestering in raft-mimicking lipid mixtures, Biophys. J. 104 (2013) 2212–2221.
[28] I. Visco, S. Chiantia, P. Schwille, Asymmetric supported lipid bilayer formation via methyl-β-cyclodextrin mediated lipid exchange: influence of asymmetry on lipid dynamics and phase behavior, Langmuir 30 (2014) 7475–7484.
[29] L.A. Clifton, M.W.A. Skoda, E.L. Daulton, A.V. Hughes, A.P. Le Brun, J.H. Lakey, S.A. Holt, Asymmetric phospholipid: lipopolysaccharide bilayers; a gram-negative bacterial outer membrane mimic, J. R. Soc. Interface 10 (2013).
[30] L.A. Clifton, S.A. Holt, A.V. Hughes, E.L. Daulton, W. Arunmanee, F. Heinrich, S. Khalid, D. Jefferies, T.R. Charlton, J.R.P. Webster, C.J. Kinane, J.H. Lakey, An accurate in vitro model of the E. Coli envelope, Angew. Chem. Int. Ed. 54 (2015) 11952–11955.
[31] P. Schoch, D. Sargent, Surface-potentials of asymmetric charged lipid bilayers, Experientia 32 (6) (1976) 811-811.
[32] R. Latorre, J.E. Hall, Dipole potential measurements in asymmetric membranes, Nature 264 (1976) 361–363.
[33] O. Alvarez, R. Latorre, Voltage-dependent capacitance in lipid bilayers made from monolayers, Biophys. J. 21 (1978) 1–17.
[34] P. Schoch, D.F. Sargent, R. Schwyzer, Capacitance and conductance as tools for the measurement of asymmetric surface potentials and energy barriers of lipid bilayer membranes, J. Membr. Biol. 46 (1979) 71–89.
[35] Y.A. Chizmadzhev, I.G. Abidor, Bilayer lipid membranes in strong electric fields, J. Electroanal. Chem. Interfacial Electrochem. 116 (1980) 83–100.
[36] V.V. Cherny, V.S. Sokolov, I.G. Abidor, Determination of surface charge of bilayer lipid membranes, J. Electroanal. Chem. Interfacial Electrochem. 116 (1980) 413–420.
[37] M.D. Collins, S.L. Keller, Tuning lipid mixtures to induce or suppress domain formation across leaflets of unsupported asymmetric bilayers, Proc. Natl. Acad. Sci. 105 (2008) 124–128.
[38] M. Montal, P. Mueller, Formation of bimolecular membranes from lipid monolayers and a study of their electrical properties, Proc. Natl. Acad. Sci. U. S. A. 69 (1972) 3561–3566.
[39] Y. Gerelli, L. Porcar, L. Lombardi, G. Fragneto, Lipid exchange and flip-flop in solid supported bilayers, Langmuir 29 (2013) 12762–12769.
[40] K. Funakoshi, H. Suzuki, S. Takeuchi, Lipid bilayer formation by contacting monolayers in a microfluidic device for membrane protein analysis, Anal. Chem. 78 (2006) 8169–8174.
[41] H. Bayley, B. Cronin, A. Heron, M.A. Holden, W.L. Hwang, R. Syeda, J. Thompson, M. Wallace, Droplet interface bilayers, Mol. BioSyst. 4 (2008) 1191–1208.
[42] M.A. Holden, D. Needham, H. Bayley, Functional bionetworks from nanoliter water droplets, J. Am. Chem. Soc. 129 (2007) 8650–8655.
[43] W.L. Hwang, M. Chen, B. Cronin, M.A. Holden, H. Bayley, Asymmetric droplet interface bilayers, J. Am. Chem. Soc. 130 (2008) 5878–5879.
[44] W.L. Hwang, M. Chen, B.D. Cronin, M.A. Holden, H. Bayley, Asymmetric droplet Interface bilayers, J. Am. Chem. Soc. 130 (2008) 5878–5879.
[45] Y. Elani, X. Niu, O. Ces, Novel technologies for the formation of 2-D and 3-D droplet interface bilayer networks, Lab Chip 12 (2012) 3514–3520.
[46] P.J. Milianta, M. Muzzio, J. Denver, G. Cawley, S. Lee, Water permeability across symmetric and asymmetric droplet Interface bilayers: interaction of cholesterol sulfate with DPhPC, Langmuir 31 (2015) 12187–12196.
[47] N.E. Barlow, E. Smpokou, M.S. Friddin, R. Macey, I.R. Gould, C. Turnbull, A.J. Flemming, N.J. Brooks, O. Ces, L.M.C. Barter, Engineering plant membranes using droplet interface bilayers, Biomicrofluidics 11 (2017) 024107.
[48] N.E. Barlow, G. Bolognesi, S. Haylock, A.J. Flemming, N.J. Brooks, L.M.C. Barter, O. Ces, Rheological droplet Interface bilayers (rheo-DIBs): probing the unstirred water layer effect on membrane permeability via spinning disk induced shear stress, Sci. Rep. 7 (2017) 17551.
[49] E.C. Freeman, J.S. Najem, S. Sukharev, M.K. Philen, D.J. Leo, The mechanoelectrical response of droplet interface bilayer membranes, Soft Matter 12 (12) (2016) 3021–3031.
[50] J. Hall, Voltage-dependent lipid flip-flop induced by alamethicin, Biophys. J. 33 (1981) 373–381.
[51] S. Toyama, A. Nakamura, F. Toda, Measurement of voltage dependence of capacitance of planar bilayer lipid membrane with a patch clamp amplifier, Biophys. J. 59 (1991) 939–944.
[52] M.-A. Nguyen, B. Srijanto, C.P. Collier, S.T. Retterer, S.A. Sarles, Hydrodynamic trapping for rapid assembly and in situ electrical characterization of droplet interface bilayer arrays, Lab Chip 16 (2016) 3576–3588.
[53] A. Yasmann, S. Sukharev, Properties of diphytanoyl phospholipids at the air–water Interface, Langmuir 31 (2014) 350–357.
[54] I. Vodyanoy, J. Hall, T. Balasubramanian, Alamethicin-induced current-voltage curve asymmetry in lipid bilayers, Biophys. J. 42 (1983) 71–82.
[55] G.J. Taylor, S.A. Sarles, Heating-enabled formation of droplet Interface bilayers using *Escherichia coli* total lipid extract, Langmuir 31 (2015) 325–337.
[56] G.J. Taylor, G.A. Venkatesan, C.P. Collier, S.A. Sarles, Direct in situ measurement of specific capacitance, monolayer tension, and bilayer tension in a droplet interface bilayer, Soft Matter 11 (2015) 7592–7605.
[57] G.J. Taylor, F.A. Heberle, J.S. Seinfeld, J. Katsaras, C.P. Collier, S.A. Sarles, Capacitive detection of low-enthalpy, higher-order phase transitions in synthetic and natural composition lipid membranes, Langmuir 33 (2017) 10016–10026.
[58] B. Zheng, J.D. Tice, R.F. Ismagilov, Formation of droplets of alternating composition in microfluidic channels and applications to indexing of concentrations in droplet-based assays, Anal. Chem. 76 (2004) 4977–4982.
[59] C. Usai, C. Marchetti, F. Gambale, M. Robello, A. Gorio, Capacitance—voltage relationship in phospholipid bilayers containing gangliosides, FEBS Lett. 153 (1983) 315–319.
[60] M. Mottamal, T. Lazaridis, Voltage-dependent energetics of alamethicin monomers in the membrane, Biophys. Chem. 122 (2006) 50–57.
[61] H.W. Huang, Y. Wu, Lipid-alamethicin interactions influence alamethicin orientation, Biophys. J. 60 (1991) 1079–1087.
[62] K. He, S.J. Ludtke, W.T. Heller, H.W. Huang, Mechanism of alamethicin insertion into lipid bilayers, Biophys. J. 71 (1996) 2669–2679.
[63] S. Stankowski, U.D. Schwarz, G. Schwarz, Voltage-dependent pore activity of the peptide alamethicin correlated with incorporation in the membrane: salt and cholesterol effects, Biochim. Biophys. Acta Biomembr. 941 (1988) 11–18.
[64] J.S. Allhusen, J.C. Conboy, The ins and outs of lipid flip-flop, Acc. Chem. Res. 50 (2017) 58–65.
[65] Z. Chen, R. Rand, The influence of cholesterol on phospholipid membrane curvature and bending elasticity, Biophys. J. 73 (1997) 267.
[66] Z. Chen, R.P. Rand, Comparative study of the effects of several n-alkanes on phospholipid hexagonal phases, Biophys. J. 74 (1998) 944–952.
[67] G.A. Venkatesan, G.J. Taylor, C.M. Basham, N.G. Brady, C.P. Collier, S.A. Sarles, Evaporation-induced monolayer compression improves droplet interface bilayer formation using unsaturated lipids, Biomicrofluidics 12 (2018) 024101.
[68] K. He, S.J. Ludtke, W.T. Heller, H.W. Huang, Mechanism of alamethicin insertion into lipid bilayers, Biophys. J. 71 (1996) 2669–2679.
[69] I. Vodyanoy, J.E. Hall, T.M. Balasubramanian, Alamethicin-induced current-voltage curve asymmetry in lipid bilayers, Biophys. J. 42 (1983) 71–82.
[70] A.J. Krauson, J. He, W.C. Wimley, Determining the mechanism of membrane permeabilizing peptides: identification of potent, equilibrium pore-formers, Biochim. Biophys. Acta 1818 (2012), https://doi.org/10.1016/j.bbamem.2012.1002.1009.
[71] W.C. Wimley, S.H. White, Determining the membrane topology of peptides by fluorescence quenching, Biochemistry 39 (2000) 161–170.
[72] J.E. Hall, Voltage-dependent lipid flip-flop induced by alamethicin, Biophys. J. 33 (1981) 373–381.
[73] M.K. Mathew, P. Balaram, A helix dipole model for alamethicin and related transmembrane channels, FEBS Lett. 157 (1983) 1–5.
[74] G. Schwarz, H. Gerke, V. Rizzo, S. Stankowski, Incorporation kinetics in a membrane, studied with the pore-forming peptide alamethicin, Biophys. J. 52 (1987) 685–692.
[75] V. Rizzo, S. Stankowski, G. Schwarz, Alamethicin incorporation in lipid bilayers: a thermodynamic study, Biochemistry 26 (1987) 2751–2759.
[76] G. Schwarz, S. Stankowski, V. Rizzo, Thermodynamic analysis of incorporation and aggregation in a membrane: application to the pore-forming peptide alamethicin, Biochim. Biophys. Acta Biomembr. 861 (1986) 141–151.